Sensors and Materials, Vol. 37, No. 7 (2025) 2877–2907
MYU Tokyo

S & M 4092

Comparative Analysis of Improved Mahalanobis–Taguchi System and Convolutional Neural Networks for Car Window Motor Sound Recognition

Chin-Yi Cheng*

Department of Mechanical Engineering, National Yunlin University of Science and Technology, Douliu, Yunlin 64002, Taiwan

(Received January 16, 2025; accepted May 7, 2025)

Keywords: motor for electric sunroof, sound recognition, Mahalanobis–Taguchi System (MTS), convolutional neural networks (CNNs)

In this study, we conducted a comparative evaluation of an enhanced Mahalanobis–Taguchi system (MTS) and convolutional neural networks (CNNs) for the recognition of acoustic signals, concentrating on the diagnostic monitoring of automotive window motors. The enhanced MTS integrates sophisticated feature selection and optimized Mahalanobis distance computations to improve anomaly detection using a specified sound quality index. High-resolution acoustic data were acquired utilizing dual high-sensitivity microphones to ensure reliable input for both methodologies. The CNN framework, enhanced by Long Short-Term Memory units and multiscale feature extraction, attained an accuracy greater than 96.6%. This performance notably exceeded that of the MTS, particularly in modeling intricate acoustic signal variations. Although the MTS provides statistical precision, it demonstrates reduced efficacy in managing subtle variability as opposed to adaptive CNN-based models. In this research, we elucidated the essential trade-offs between conventional and machine learning approaches, providing insights for choosing optimal acoustic monitoring methodologies within automotive applications.

1. Introduction

Acoustic elements play a pivotal role in affecting consumer perceptions regarding the quality and craftsmanship of passenger vehicles.(1,2) The auditory characteristics of a vehicle, encompassing operational sounds, are frequently regarded as indicators of overall structural quality.(3,4) Consumers generally correlate low noise levels and a serene acoustic environment with superior craftsmanship, a perception particularly relevant to electric vehicles (EVs), which are distinguished by their minimal engine vibrations and low sound frequencies.(5–7) Nonetheless, the nearly silent operation of EVs presents new challenges, as other mechanical noises—such as those emanating from car window motors—become more prominent and can lead to customer dissatisfaction. As noted by Bhosale *et al.*, Buzz, Squeak and Rattle (BSR) are commonly classified as vehicle quality issues and marked under Noise, Vibration, and Harshness

*Corresponding author: e-mail: zezheng@yuntech.edu.tw
https://doi.org/10.18494/SAM5548

ISSN 0914-4935 © MYU K.K.
https://myukk.org/

(NVH).(8,9) Mitigating these issues can be particularly complex owing to the intricate mechanisms and assemblies involved. Abnormal motor noises, including squeaks and rattles (S&R), typically caused by the relative movement of components or impacts from loose joints, detrimentally impact customer satisfaction and the perceived quality of the vehicle.(10,11) The configuration of the electric motor and transmission mechanism is illustrated in Fig. 1. The electric sunroof employs a permanent magnet DC motor for automated opening/closing and positional adjustment. The sunroof's drive mechanism facilitates the opening and closing, as well as angle adjustment, following the motor's deceleration through the worm gear system.

Recent research has substantially advanced acoustic monitoring technologies pertinent to automotive diagnostics, employing machine learning, statistical methodologies, and spectral analysis to enhance fault detection and predictive maintenance.(12–14) Deep learning models, specifically convolutional neural networks (CNNs), have been utilized to classify vehicles on the basis of audio signals with considerable precision.(15) This approach is further enhanced through the use of time-frequency visualizations such as spectrograms and scalograms, which capture distinct acoustic patterns of different vehicle types, as illustrated in Fig. 2.(16)

Recent research has emphasized the importance of acoustic signals in evaluating vehicle quality and diagnosing faults in mechanical systems. Studies on EV components have focused on reducing noise through vibration analysis and material optimization.(17–20) In smart robotics, vision-based inspection techniques have been applied to enhance grasping performance, while deep learning models, particularly convolutional and recurrent neural network (CNN-RNN) architectures, have been employed for predictive maintenance in motor drive control systems.(21,22) Recent progress in acoustic monitoring technologies has markedly improved fault detection and predictive maintenance in DC motor drives used in industrial robotics. Diverse methodologies, encompassing deep learning models such as CNNs-RNNs, statistical techniques, and spectral analysis, have been utilized to enhance diagnostic precision and system reliability.(23) These advances highlight the convergence of acoustics, AI, and sensor fusion in enabling intelligent mobility and automated diagnostic solutions. The AI mechanic system has further exemplified the ability to diagnose faults directly from raw audio data, underscoring the potential of machine-learning-driven acoustic analysis within industrial contexts.(24)

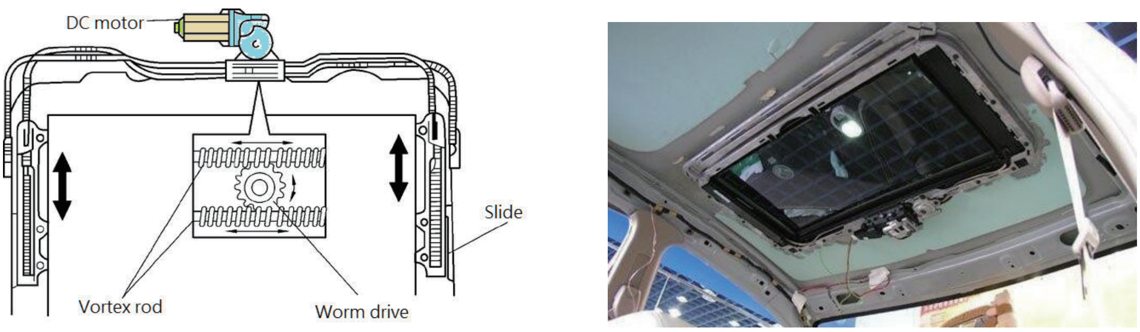

Fig. 1. (Color online) Structural diagram of transmission mechanism of automobile electric window (sunroof).

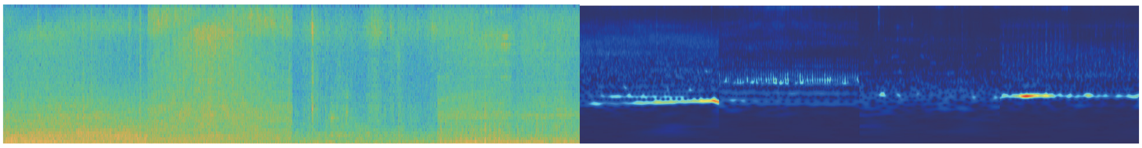

Fig. 2. (Color online) Spectrogram features for (a) car, (b) motorcycle, (c) no traffic, and (d) truck, corresponding to the labeled acoustic data segments.

Audio-based anomaly detection has been widely applied beyond industrial robotics, including railway and automotive systems. Techniques such as Mel-frequency cepstral coefficients (MFCCs) combined with Support Vector Machines (SVMs) have shown high accuracy in fault detection, highlighting the value of low-cost, nonintrusive acoustic monitoring for predictive maintenance.(25) In complex industrial environments, recent studies using Variational Mode Decomposition (VMD)-SVM achieved an accuracy of 95.8% in diagnosing faults in car folding rearview mirrors, as shown in Fig. 3.

Acoustic disturbances within vehicles, exemplified by suspension damper noise, substantially affect perceptions of consumer quality. In response, a noise identification method employing the Genetic Algorithm-SVM was introduced, improving diagnostic precision through the analysis of attribute correlations derived from vehicle testing.(26–28) Furthermore, the application of wavelet packet transform for signal decomposition was utilized to enhance noise recognition. Figure 4 shows the road test configuration, where recordings were made at specified locations for each shock absorber sample, capturing both internal noise and vibration signals.

Precise fault diagnosis is imperative for the reliable performance of electromechanical systems, but data acquisition remains a formidable challenge owing to the complexity of these systems. Conventional sensor-based methods are often intrusive and financially burdensome. Conversely, acoustic monitoring presents a noninvasive, efficient alternative through the analysis of machine-generated sounds. Techniques such as modulation signal analysis have been demonstrated to be effective for monitoring gearboxes, alongside machine learning models such as random forests and neural networks that facilitate predictive maintenance. However, obstacles such as noise interference, restricted data availability, and complex acquisition procedures persist, impeding wider implementation.(29,30) In this investigation, we aim to improve vehicle reliability and safety through the application of advanced diagnostic techniques grounded in acoustic analysis, and to conduct a comparative evaluation of the Mahalanobis–Taguchi system (MTS) and CNNs for the detection of anomalies in the acoustics of car window motors. The MTS is particularly well suited to scenarios characterized by limited labeled fault data, offering high diagnostic precision with minimal data input; this is advantageous in contexts where fault data are scarce. In contrast, CNNs exhibit remarkable capability to discern complex patterns within high-dimensional data, making them effective for the analysis of subtle variations in motor noise. Recognizing that these acoustics encompass both structured and unstructured signals, we investigated how each methodology manages this complexity. Taking advantage of the strengths of both methodologies, we provide information on the selection of the most appropriate model for automotive acoustic diagnostics. The choice of the MTS and CNNs is supported by their proven efficacy in quality control, anomaly detection, and sound recognition

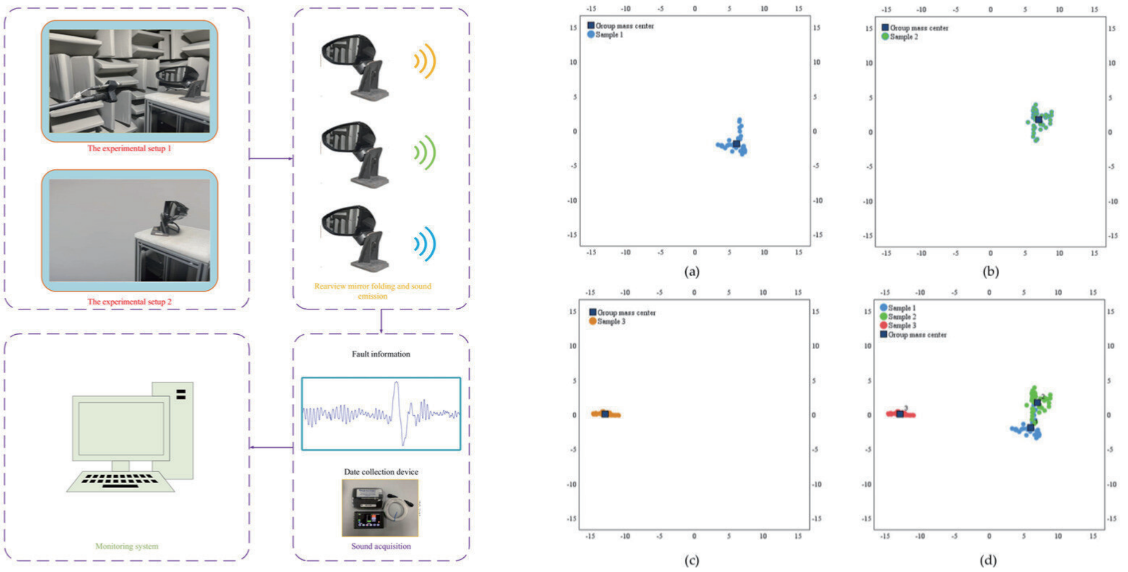

Fig. 3. (Color online) Two setups: a semi-muffled laboratory (setup 1) and a standard laboratory (setup 2). Panels (a)–(c) display the distribution of selected Intrinsic Mode Functions (IMFs) for samples 1–3, whereas panel (d) shows their collective distribution. The x- and y-axes represent two discriminant functions.(31)

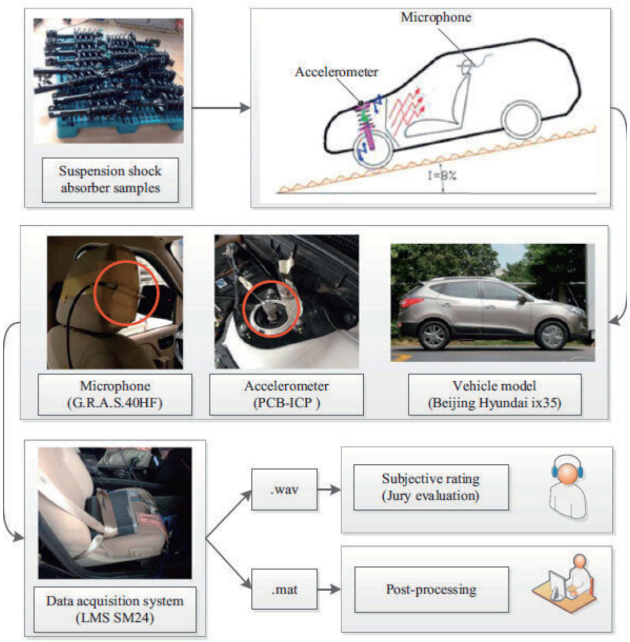

Fig. 4. (Color online) Vehicular road test for the identification of suspension shock absorber S&R noise.(32)

in various engineering disciplines. The MTS, as conceived by Genichi Taguchi, demonstrates outstanding effectiveness in diagnosing and forecasting outcomes using multivariate data, thereby facilitating significant improvements in product and process quality.(33) As indicated by Peng *et al.*, the MTS has displayed superior performance compared with logistic regression and neural networks within the tablet PC manufacturing sector, achieving a predictive capacity of 98% while simultaneously reducing the number of test items, thus lowering testing durations, personnel requirements, and equipment costs.(24) Within the electrical and electronics industry, the MTS has been instrumental in optimizing production processes, identifying critical parameters, and minimizing product rejection rates.(25) In contrast, CNNs, owing to their advanced deep learning structures, excel in analyzing complex data patterns. For example, Jung *et al.* conducted a study in which CNNs proficiently diagnosed rotor faults, demonstrating the model's capability to accurately identify failures across various normal and faulty sound scenarios within the system. The accuracy of training and validation exceeded 99%, even when limited datasets were restricted.(29)

The MTS is a well-established method widely used for pattern recognition and diagnostic applications, particularly effective for small datasets with sequential patterns. However, as an older method, the MTS has limitations in handling complex and high-dimensional data, such as intricate acoustic patterns. To address this, we enhanced the MTS by incorporating an optimized feature selection process and improved Mahalanobis distance (*MD*) calculations, aiming to increase its diagnostic accuracy and robustness. These enhancements make the MTS suitable for capturing temporal relationships in car window motor sound data, aiding in the identification of fault-related patterns.

CNNs represent a contemporary methodology for fault diagnosis, proficiently managing complex, high-dimensional data. By incorporating multiscale feature extraction techniques (Conv1D, Conv2D, and LSTM) alongside preprocessing methods such as MFCCs and short-time Fourier transform (STFT), CNNs transform acoustic signals into spectrograms tailored for the detection of motor faults. The acquisition of high-quality data is achieved by the utilization of dual high-sensitivity microphones within a soundproof environment. Conversely, the enhanced MTS employs an advanced *MD*-based health index for the identification of anomalies within smaller datasets. In this study, we present a comparison between the MTS and CNN approaches, highlighting the data efficiency of the MTS and the capability of CNNs in analyzing complex signals. This integrated perspective offers a comprehensive solution for automotive fault detection and supports the development of more practical diagnostic tools.

2. Methodology

2.1 Data collection and acoustic signal acquisition

After the data acquisition phase, the dataset was systematically structured with metadata pertaining to the operating conditions and observed anomalies to facilitate robust model training and validation. Although initial fast Fourier transform (FFT) analyses revealed frequency patterns associated with faults, they exhibited deficits in sensitivity to amplitude fluctuations. To address this limitation, MFCCs were extracted, which offered enhanced spectral and temporal characteristics, thus markedly increasing the precision of the CNN training and diagnostic. Figure 5 shows an automated inspection system that employs sound spectrogram analysis to identify atypical acoustic emissions in automobile window motors during the manufacturing

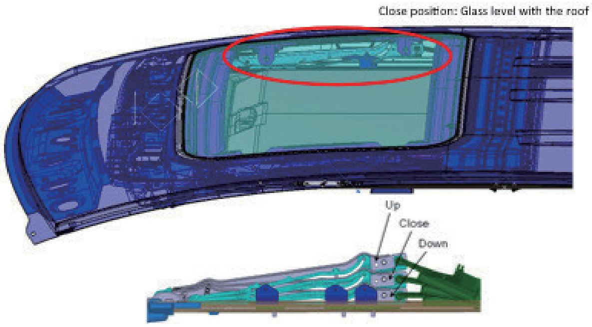

(a)

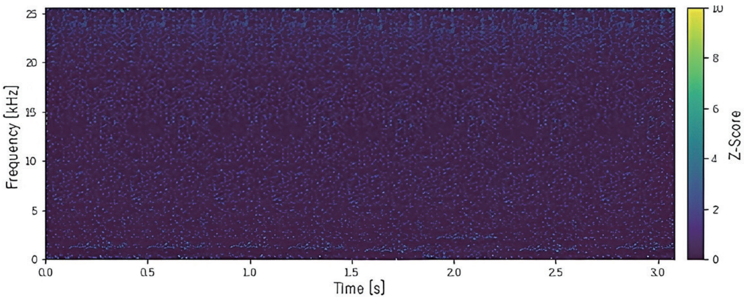

(b)

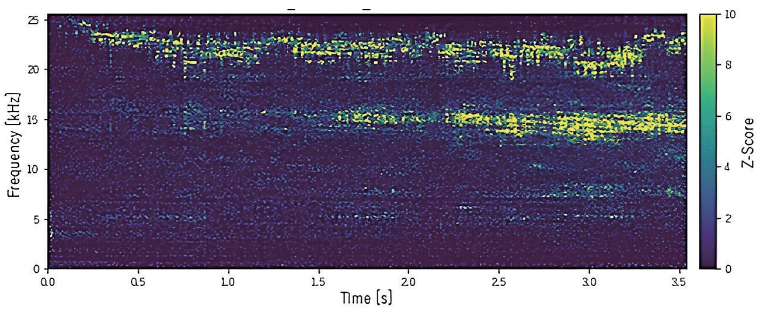

(c)

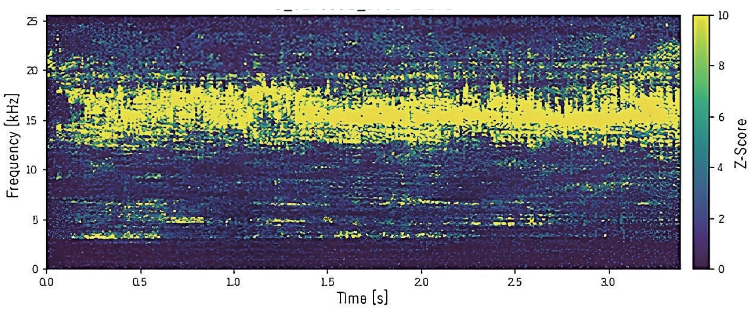

(d)

Fig. 5. (Color online) (a) Automated inspection system for detecting abnormal sounds in car window motors based on spectrogram analysis. (b) Standard sound model. (c) NG item—Squeaking sound. (d) NG item—Zizi sound.

process. A microphone is strategically placed within the sliding roof rail to effectively capture mechanical and frictional noises during operation, thus improving the precision of anomaly detection. The system conducts a comparative analysis of spectrograms from both standard and defective (NG) products. Standard spectrograms exhibit a consistent frequency distribution, whereas NG spectrograms demonstrate variations in intensity (e.g., yellow-green regions), which serve as indicators of anomalies such as friction (squeaking) or internal vibrations (zizi sounds). Anomalies within the system are identified through variations in the colorations of the spectrogram, wherein more intense colorations signify greater irregularities. With a missed detection rate of 0% and an approximately false detection rate of 5%, the system exhibits high levels of accuracy and sensitivity. Consequently, it offers a reliable and noninvasive instrument for the acoustic diagnosis of faults and the assurance of quality within the manufacturing process.

Figure 6 shows the smart window motor sound recognition system implemented via a multi-time series. The procedure commences with the application of voltage to the motor, resulting in sound generation that is captured by dual high-sensitivity microphones. These signals undergo processing to facilitate feature extraction, followed by the computation of the *MD* health index. The *MD* was preferred over deep learning methodologies owing to its efficacy with limited datasets, its ability to operate in real time, and the simplicity of interpretation. The *MD* health index integrates various sound metrics into a single value, enabling rapid anomaly detection. By contrasting current data with a reference set, the system discerns deviations that may indicate potential motor malfunctions. This streamlined, automated methodology improves diagnostic precision and enhances quality control within the context of automotive manufacturing.

Audio signals are captured using two directional microphones, one for motor noise and the other for ambient sound. A 10 s hiatus in acquisition facilitates data storage, adaptive filtering,

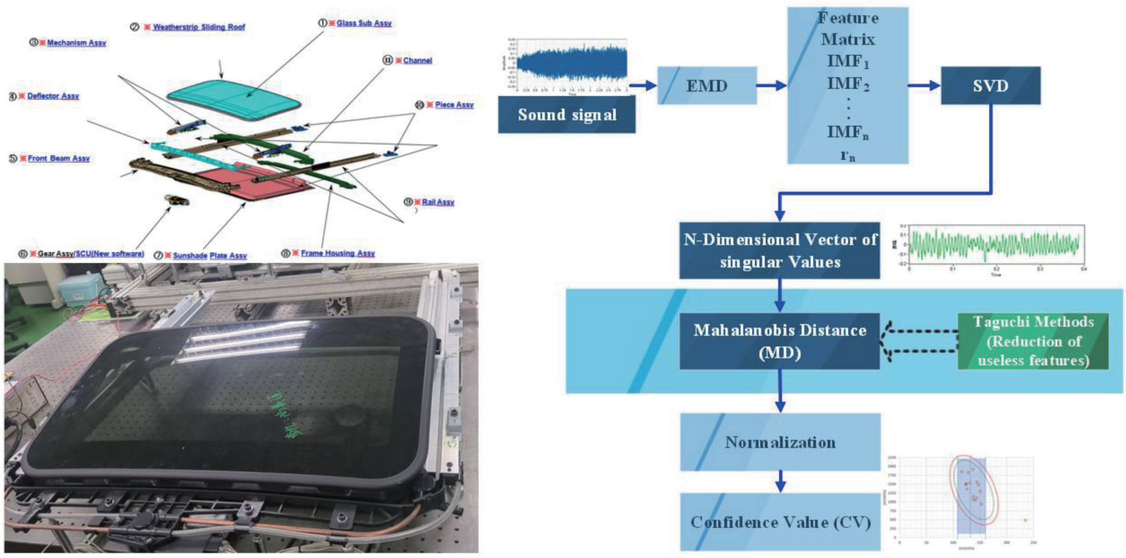

Fig. 6. (Color online) Smart window motor sound recognition system flow chart using MTS.

frame segmentation, and frequency phase classification, culminating in refined frequency charts and maps. Multiscale volume analysis is performed using Conv1D, Conv2D, and LSTM models. Feature selection is optimized by recursive feature elimination (RFE), chi-square (χ^2) test, and variance analysis. As shown in Fig. 7, the procedure is initiated by applying voltage to the motor, which in turn triggers the capture of the sound. The audio data undergo preprocessing through MFCCs, are transformed into spectrograms, and are subsequently inputted into CNN models incorporating LSTM layers for precise anomaly detection.

2.2 Design of soundproof enclosure and sensor configuration

The precise diagnosis of motor faults in automotive window systems requires the use of high-quality acoustic data, which, in turn, demands precise instrumentation and controlled conditions. Acoustic emission is proven to be particularly effective for the detection of faults, leaks, and material fatigue. Figures 8 and 9 illustrate the development of a custom soundproof enclosure (180 × 300 × 180 mm^3) equipped with premium insulation and a high-sensitivity directional microphone designed to ensure clear and undistorted recordings. The HTT-006 DC motor (DC+12V) was subjected to tests under various loads and speeds, facilitating the comparison of normal and abnormal acoustic patterns. Environmental factors such as temperature, humidity, and resonance were meticulously controlled. Data acquisition was performed using LabVIEW, with recordings stored in WAV format. The preprocessing stage involved noise reduction and spectral analysis, which served to enhance signal clarity and improve diagnostic accuracy and repeatability within automotive applications.

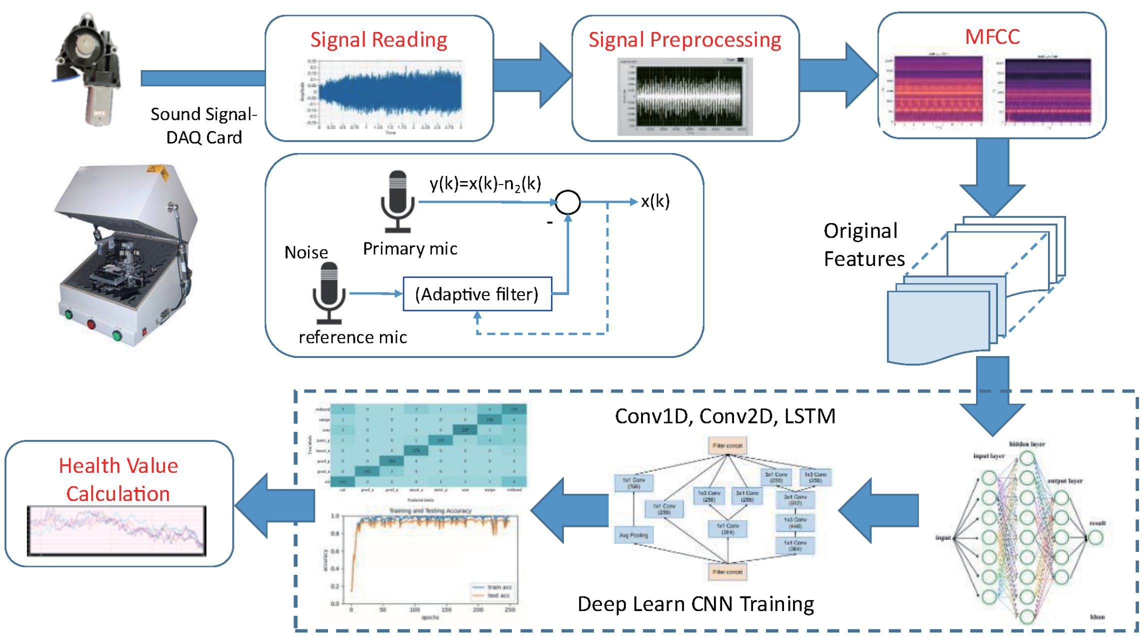

Fig. 7. (Color online) Smart window motor sound recognition system flow chart using CNNs.

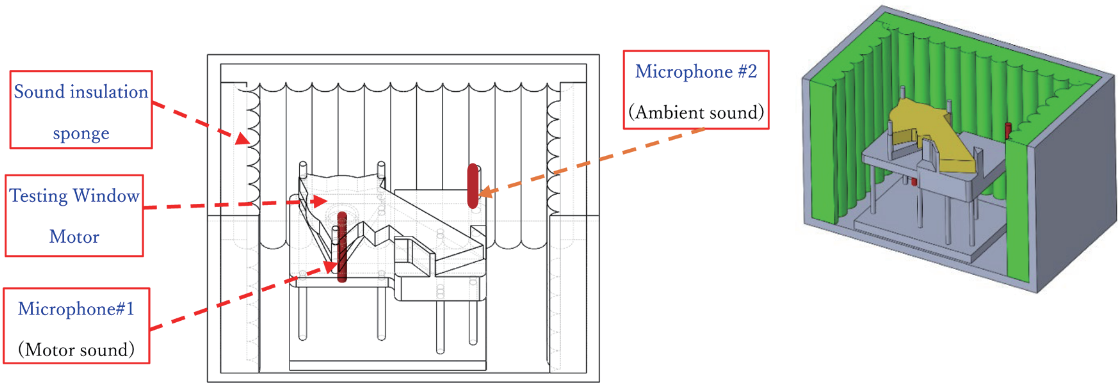

Fig. 8. (Color online) Smart window motor identification and testing equipment platform design architectural diagram.

Fig. 9. (Color online) Soundproof box entity diagram.

The HTT-006 DC motor operates at a rated DC +12 V and supports both forward and reverse rotation capabilities. This motor is utilized primarily in electric sunroof systems, in which a permanent magnet DC motor enables the automated opening, closing, and angular adjustment of the sunroof through a worm gear and transmission mechanism. Under normal operating conditions, the motor produces electromagnetic and mechanical noises, predominantly within the frequency range of 200 Hz to 2 kHz. The main sources of these noises include interactions between brushes and commutators, gear engagement, and structural vibrations. Abnormal sound patterns are illustrated in Table 1. The setup of the window motor acoustic monitoring platform, as shown in Fig. 10.

2.3 Microphone configuration and signal conditioning

In this study, the sound acquisition process utilized the PCB Model 130F21 microphone, which is recognized for its exceptional sensitivity and stability. This microphone plays a pivotal role in the precise recording of sound signals originating from car window motors. Table 2 outlines the main specifications and operational characteristics of the microphone. The Model

Table 1
(Color online) Physical diagram of permanent magnet DC motor power window (sunroof).

Fault type	Acoustic signature	Frequency range
Bearing wear or misalignment	Increased low-frequency vibrations	~200–800 Hz
Gear meshing issues (backlash, wear, or improper lubrication)	High-frequency tonal noise	~1 kHz–3 kHz
Excessive friction or foreign object interference	Broadband noise	Beyond 3 kHz

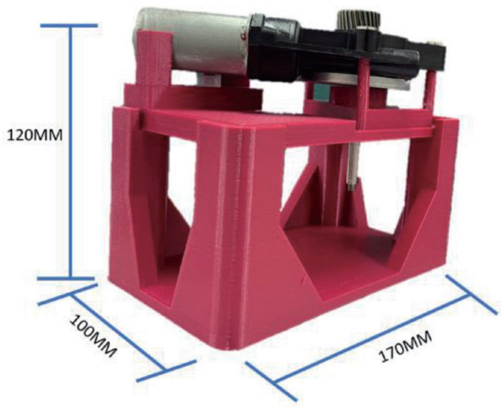

Fig. 10. (Color online) Real-world setup of the window motor acoustic monitoring platform.

Table 2
(Color online) PCB Model 130F21 specification sheet.[30]

Performance	Description
Nominal microphone diameter	1/4"
Frequency response	10 to 20000 Hz
Sensitivity	45 mV/Pa
Inherent noise (A-weighted)	< 26 dB(A) re 20 μPa
Dynamic range (3% distortion limit)	> 122 dB re 20 μPa
Excitation voltage	18 to 30 VDC
Constant current excitation	2 to 20 mA

130F21 microphone is integrated with an integrated electronics piezo-electric (IEPE) circuit, designed to transform the high-impedance charge signal from the piezoelectric element into a low-impedance voltage signal (approximately 100 Ω). This circuit further facilitates constant current excitation ranging from 2 to 20 mA, thereby maintaining signal integrity throughout extended cable lengths and ensuring sound measurement reliability with minimal degradation. For the accurate capture of motor acoustics, the microphone was strategically placed directly beneath the motor body, an optimal position that reduces external noise interference and accurately apprehends the authentic acoustic signature of the motor during operation.

2.4 Signal acquisition system: microphone and ADC module configuration

We used the PCB 130F21 microphone in conjunction with the ADLINK USB-2405 data acquisition module, as shown in Table 3. USB-2405, equipped with a 24-bit Sigma-Delta ADC and an anti-aliasing filter, enabled the high-resolution processing of acoustic signals. Operated at a sampling rate of 48 kHz with a cutoff frequency of 24 kHz, it preserved high-frequency components crucial for detecting motor faults. The filter effectively mitigated noise while maintaining essential spectral characteristics. Its four-channel input, AC/DC coupling, and automatic calibration enhanced data accuracy. Figures 11(a) and 11(b) illustrate the motor signals of GO and NO GO, where the NG spectrograms demonstrate spectral disturbances—particularly above 1024 Hz—supporting the efficacy of MTS and CNN fault detection. The observed interference is primarily attributed to the looseness of internal components, resulting in impact noise. Even minor assembly defects can lead to atypical acoustic behavior during motor operation. To validate this, a quantitative analysis of frequency variations and power spectral

Table 3
(Color online) ADLINK USB-2405 sound and vibration input module.

	Hi-Speed USB 2.0, powered by USB bus 24-bit Sigma-Delta ADC with built-in anti-aliasing filter Four-channel simultaneous sampled analogue inputs up to 128 kS/s Analogue and digital triggering and full autocalibration AC or DC input coupling, software selectable

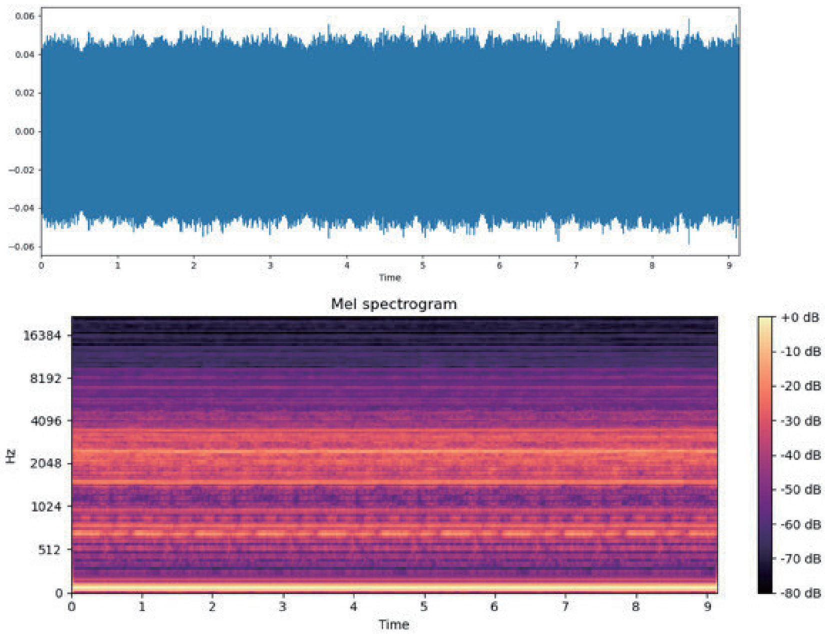

(a)

Fig. 11. (Color online) (a) GO and (b) NG sample audio signals of motor sound captured in the time and time-frequency domains.

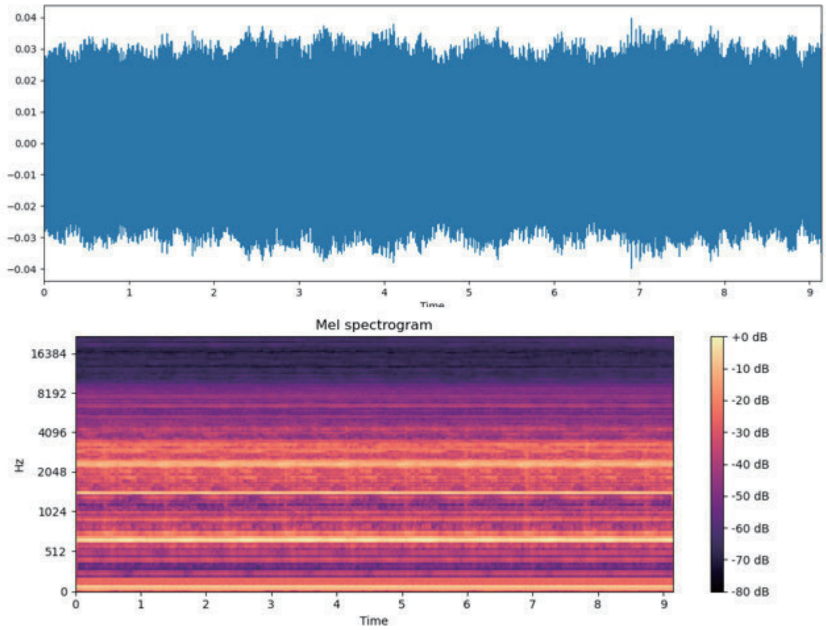

(b)

Fig. 11. (Continued) (Color online) (a) GO and (b) NG sample audio signals of motor sound captured in the time and time-frequency domains.

density (PSD) was performed to characterize anomalies in NG motors. As shown in Fig. 12, (a) corresponds to GO and (b) to NG. The pronounced PSD peaks in the NG signal indicate the presence of abnormal frequencies arising from mechanical noise or irregular vibrations, thereby effectively distinguishing faulty from normal functioning. The GO motor exhibits a maximum PSD of −57.67 dB/Hz, in contrast to −66.62 dB/Hz for the NG motor. The increased PSD in the GO motor signifies higher energy at the expected frequencies, whereas the decreased PSD in the NG motor suggests mechanical defects. This comparison affirms the efficacy of the proposed method in accurately detecting motor abnormalities.

To improve data quality and optimize model performance, the raw sound recordings were divided into 1 s segments. Each motor underwent a recording session lasting 10 s over 40 separate sessions, culminating in a total of 16000 samples, covering both forward and reverse rotational directions. The dataset was methodically partitioned into 70% for training (11200 samples) and 30% for testing (4800 samples) to ensure balanced learning. To increase the signal integrity of MEMS microphones, salt-and-pepper noise was mitigated using a sliding median filter, while overload distortion was addressed via an adaptive threshold algorithm. These preprocessing measures effectively preserved essential acoustic characteristics and improved diagnostic reliability.

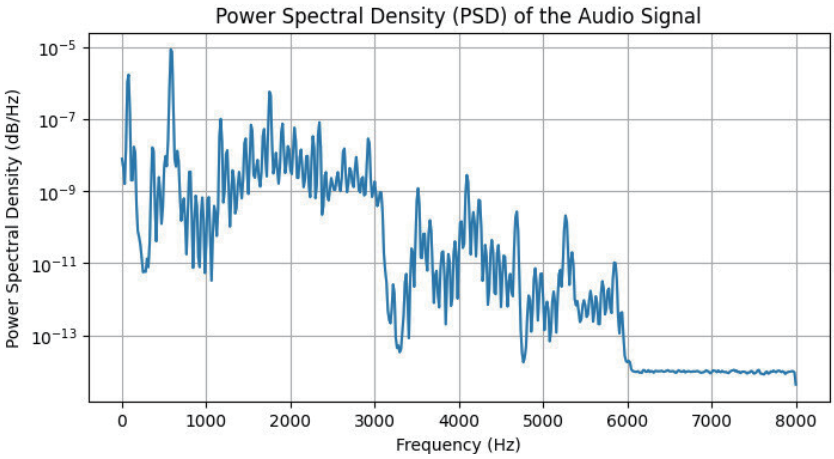

(a)

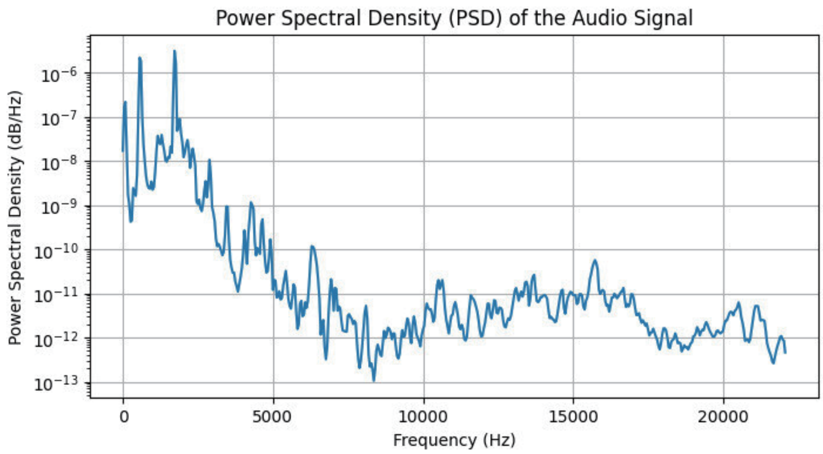

(b)

Fig. 12. (Color online) (a) GO and (b) NG PSD values of the operation sound of the sunroof motor.

3. Sound Recognition Technology for Motor Fault Diagnosis

3.1 MTS

The MTS was utilized for the classification and anomaly detection of acoustic data obtained from car window motors. In this study, enhancements were made to the MTS algorithm to improve its diagnostic precision and adaptability to intricate acoustic patterns. These enhancements comprise optimized feature extraction techniques, advanced statistical modelling, and an improved calculation of the *MD*. The refined algorithm facilitates superior differentiation between normal and abnormal acoustic profiles.

a. Feature Extraction

The initial phase of the enhanced MTS entails the extraction of a wide range of acoustic features from the recorded sound signals. Statistical features including mean, variance, skewness, and kurtosis are integrated with temporal features such as duration and frequency patterns to encapsulate the complex characteristics of motor sounds. These features are selected and weighted according to their importance for the diagnostic task, ensuring that the extracted data accurately represent the operating state of the motor. The refined algorithm automates feature ranking to prioritize those most significantly correlated with anomalies.

b. *MD*

Upon the completion of feature extraction, the *MD* is calculated for each sound sample. This metric quantifies deviations from a reference baseline formulated from a training dataset comprising normal motor sounds. In contrast to the conventional multivariate time series method, the enhanced algorithm integrates a scaled squared *MD*, which adjusts for discrepancies in feature contributions. This refinement enhances the sensitivity to identify subtle anomalies.

The formula for the squared *MD* is given as

$$MD_k^2 = \frac{1}{p} z_k^T \cdot R^{-1} \cdot z_k, \tag{1}$$

where MD_k^2 is the squared *MD* of the *k*-th sample, p is the number of features (dimensionality), z_k is the standardized feature vector for the *k*-th sample, R is the correlation matrix of the standardized samples, and R^{-1} is the inverse of the correlation matrix.

In sound recognition, the *MD* is affected by two categories of factors:

Controllable Factors (*X*) are the features derived from sound signals, such as spectral coefficients, frequency band energy, and short-term power.

Uncontrollable Factors (*Z*) are environmental noise, operator variability, and device-dependent factors (e.g., temperature and humidity).

To enhance the robustness of the *MD*, it is crucial to eliminate features that are sensitive to noise (*Z*), thereby improving the stability of the measurement. The functional relationship between the *MD* and these factors can be expressed as

$$MD = f\left(X, Z\right). \tag{2}$$

For anomaly detection, the stability of the *MD* is evaluated using the signal-to-noise ratio (*SNR*). *SNR* quantifies the strength of the signal relative to noise, defined as

$$SNR = \frac{\mu_{MD}^2}{\sigma_{MD}^2}, \tag{3}$$

where μ_{MD}^2 is the mean of the squared *MD*s (signal strength) and σ_{MD}^2 is the variance of the squared *MD*s (noise strength).

In practice, *SNR* is often expressed in decibels (dB) as

$$SNR_{dB} = 10\log_{10}\left(\frac{\mu_{MD}^2}{\sigma_{MD}^2}\right). \tag{4}$$

In sound recognition, dynamic thresholds are critical for distinguishing between normal and anomalous sounds. These thresholds can be derived from the distribution of *MD* values for normal samples.

- **Mean of *MD* values**:

$$\overline{x}_{MD} = \frac{1}{n}\sum_{k=1}^{n} MD_k^2 \tag{5}$$

- **Standard deviation of *MD* values**:

$$S_{MD} = \sqrt{\frac{1}{n-1}\sum_{k=1}^{n}\left(MD_k^2 - \overline{x}_{MD}\right)^2} \tag{6}$$

The threshold is then computed as

$$\varepsilon = \overline{x}_{MD} + \sqrt{\frac{1}{1+\delta-\theta}} \cdot S_{MD}, \tag{7}$$

where $\overline{x}_{MD}$ is the mean *MD* of normal samples, S_{MD} is the standard deviation of the *MD* for normal samples, δ is the small parameter controlling sensitivity, and θ is the proportion of normal *MD* values smaller than the smallest *MD* value in anomalous samples.

3.2 MTS for anomaly detection and threshold optimization

In this study, we employed the MT method for anomaly detection by evaluating the *MD* of the acquired signals. The *MD* serves as a metric for measuring deviation from the standard reference space (unit space), and its threshold is employed to categorize signals as normal or abnormal. To improve the precision and adaptability of anomaly detection, we juxtaposed the traditional fixed threshold method ($MD = 4$) with a dynamic threshold approach based on the χ^2 distribution.

3.2.1 *MD* threshold determination

(1) Traditional Fixed Threshold Method ($MD = 4$)

A commonly used threshold in the MT method is $MD = 4$, meaning:

- If $MD \leq 4$, the data is considered normal.

- If $MD > 4$, the data is classified as abnormal, as the probability of belonging to the normal reference space becomes extremely low.

This empirical threshold is derived from statistical principles, where an *MD* value exceeding 4 suggests a high likelihood of an outlier.

(2) Improved Method: Dynamic Threshold Based on χ^2 Distribution

To enhance detection accuracy and adaptability across different datasets and operating conditions, we adopted a χ^2-distribution-based threshold setting.

- 5% significance level ($p < 0.05$): The critical threshold is set at $\chi_k^2(0.95)$, representing minor deviations.
- 1% significance level ($p < 0.01$): The threshold is set at $\chi_k^2(0.99)$, indicating significant anomalies.

By employing statistically driven confidence intervals, this method provides a more flexible and precise anomaly detection approach than the conventional fixed $MD = 4$ threshold.

3.2.2 Visualization and classification of anomalies

To evaluate the efficacy of the proposed anomaly detection framework, we performed a comparative analysis of two threshold methodologies: a fixed *MD* threshold set at 4 and a dynamic threshold derived from the χ^2 distribution. Assessment is performed using essential performance metrics:

- Green (Normal): *MD* is within the normal threshold, indicating no anomaly.
- Yellow (Minor Anomaly): *MD* exceeds the 5% significance threshold ($p < 0.05$), requiring monitoring.
- Red (Severe Anomaly): *MD* exceeds the 1% significance threshold ($p < 0.01$), signaling critical failure needing immediate action.

This visualization enhances interpretability, enabling rapid assessment and response to anomalies.

3.2.3 Validation and performance evaluation

We investigated the efficacy of anomaly detection by juxtaposing a static *MD* threshold of 4 against a dynamic χ^2-based threshold. The evaluation of performance is conducted using the essential metrics below.

- Detection Accuracy: Correctly classified normal/abnormal signals
- False Alarm Rate (FAR): Normal signals misclassified as anomalies
- Miss Rate (MR): Anomalies misclassified as normal signals

These evaluation metrics improve the adaptability of the anomaly detection framework for industrial monitoring and predictive maintenance. Figure 13 illustrates how the MTS employs the *MD* to differentiate normal and abnormal motor sounds. A comparison of fixed dynamic thresholds based on $MD = 4$ and χ^2-based dynamic thresholds assesses classification accuracy, FAR, and MDR, ensuring reliable fault detection under varying conditions.

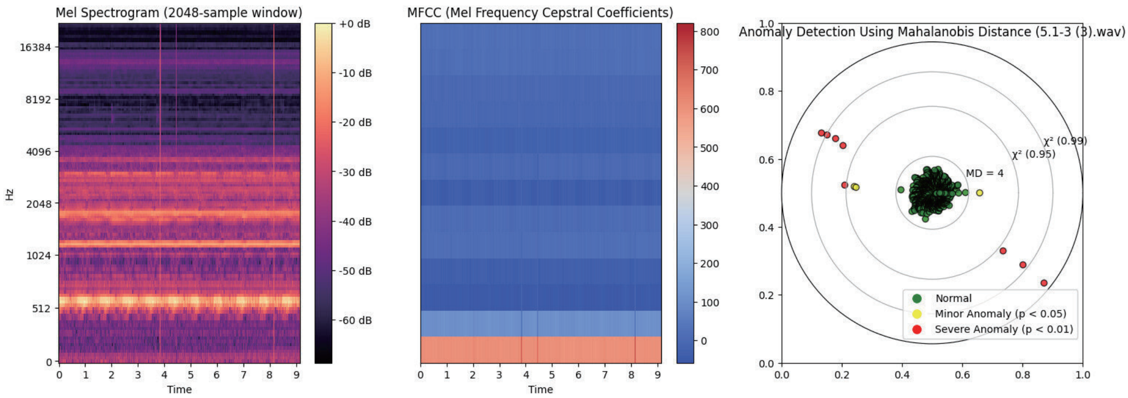

Fig. 13. (Color online) MTS for abnormal signal evaluation using *MD*.

3.3 CNNs

In this study, the experimental process for sound recognition involved a series of methodical steps designed to convert raw sound signals into meaningful features, train models, and evaluate their performance. The comprehensive procedure is as follows.

a. Preprocessing and Feature Extraction

Sound Signal Conversion: Raw sound signals from car window motors were processed into MFCCs through the following:

- Data Segmentation: Audio files were split into 70% for training and 30% for testing, ensuring a balanced dataset for evaluation.
- Feature Extraction: MFCCs were computed to capture key spectral characteristics, enabling differentiation between normal and abnormal sound patterns.

b. Preprocessing and Feature Extraction

- CNN Model Design: The model used 129 × 510 input images, with the three convolutional and pooling layers shown in Fig. 14 to process MFCC features.
- Conv1D Layers: Extracted temporal features from raw audio signals, detecting intensity and frequency variations
- Conv2D Layers: Analyzed spectrograms to identify spatial patterns and anomalies for classification
- LSTM Model Design: Captured temporal dependencies and sequential patterns in sound data shown in Fig. 15, enhancing classification accuracy

c. Proposed CNN Architecture for Motor Sound Analysis

CNNs analyze motor sound spectrograms through three Conv2D layers, each equipped with 3 × 3 kernels, a stride of 1, and the “same” padding, to facilitate the extraction of both spectral and temporal features. Each convolutional layer is succeeded by a 2 × 2 max pooling

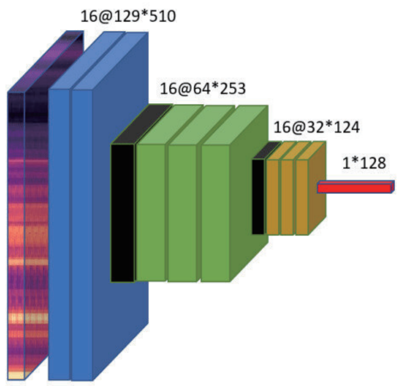

Fig. 14. (Color online) CNN model design.

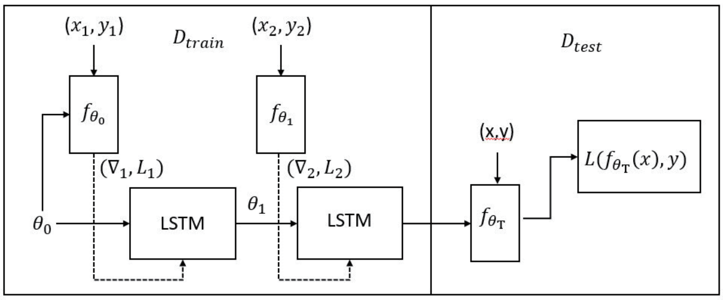

Fig. 15. LSTM model design.

layer (*stride* = 2), which serves to decrease the dimensionality and increase the computational efficiency. The CNN-LSTM architecture expands on this foundation by integrating a bidirectional long-short-term memory (Bi-LSTM) layer to capture sequential dependencies within the feature maps. Furthermore, skip connections are employed to preserve low-level feature information throughout the network. A concluding SoftMax layer performs the classification, discerning between four categories, namely, normal (forward/reverse) and abnormal (forward/reverse) motor conditions. Table 4 shows the layer configurations and output dimensions for the CNN and CNN-LSTM models.

d. Hyperparameter Tuning and Training

Hyperparameter optimization was performed through grid search with the aim of improving accuracy, precision, and recall. The model used the Adam optimizer, which began at a learning rate of 0.001 that decreased by a factor of 0.1 upon the stabilization of the validation loss over five epochs. A batch size of 32 was maintained to ensure stable convergence, with training carried out over 50 epochs. The configuration incorporated ReLU activation, cross-entropy loss, and SoftMax output, thus attaining optimal performance while mitigating overfitting.

Table 4
Comparison of CNN and CNN-LSTM model architectures with layer configurations and output shapes.

Layer (type)	Output shape	Layer (type)	Output shape
stft_input (InputLayer)	[(None, 44100, 1)]	stft_input (InputLayer)	[(None, 44100, 1)]
stft (STFT)	(None, 129, 513, 1)	stft (STFT)	(None, 138, 1025, 1)
magnitude (Magnitude)	(None, 129, 513, 1)	magnitude (Magnitude)	(None, 138, 1025, 1)
apply_filterbank	(None, 129, 512, 1)	apply_filterbank	(None, 138, 256, 1)
magnitude_to_decibel	(None, 129, 512, 1)	magnitude_to_decibel	(None, 138, 256, 1)
batch_norm	(None, 129, 512, 1)	batch_norm	(None, 138, 256, 1)
td_conv_1d_relu_1	(None, 129, 510, 8)	reshape	(None, 138, 256)
max_pool_2d_1	(None, 64, 255, 8)	td_dense_relu	(None, 138, 16)
td_conv_1d_relu_2	(None, 64, 253, 16)	bidirectional_lstm	(None, 138, 256)
max_pool_2d_2	(None, 32, 126, 16)	skip_connection	(None, 138, 272)
td_conv_1d_relu_3	(None, 32, 124, 32)	dense_1_relu	(None, 138, 64)
max_pool_2d_3	(None, 16, 62, 32)	max_pool_1d	(None, 69, 64)
dropout (Dropout)	(None, 32)	flatten (Flatten)	(None, 4416)
dense (Dense)	(None, 128)	dense_relu (Dense)	(None, 64)
softmax (Dense)	(None, 4)	softmax (Dense)	(None, 4)

e. Performance Assessment and Comparative Analysis

Following the training phase, the model was evaluated using an independent test set. Metrics such as precision and recall were used to evaluate diagnostic performance. The CNN model was contrasted with the enhanced MTS to ascertain its respective efficacies in identifying motor anomalies. To enhance auditory recognition, CNNs were integrated with FFT, STFT, and MFCCs to extract crucial spectral and temporal characteristics, thus increasing the model's ability to differentiate between normal and abnormal acoustic patterns.

f. Feature Selection Methodology

To enhance the efficacy and performance of classification, RFE alongside χ^2 analysis was utilized for feature selection. The methodology included several stages: Feature extraction: Features from both the time and frequency domains, such as MFCCs, spectral centroid, zero-crossing rate, and short-time energy, were extracted to effectively represent motor acoustics. Statistical Evaluation: The χ^2 test facilitated the identification of features that demonstrated substantial relevance to classification labels, thereby enabling the elimination of less significant features to increase robustness and mitigate overfitting.

3.4 FFT

FFT is a fundamental technique for converting time-domain sound signals into frequency-domain sound signals. This transformation reveals the frequency components of the sound, which is critical for understanding its spectral characteristics. The FFT formula is given by

$$A[K] = \sum_{n=0}^{N-1} W_N^{kn} \cdot a[n], \quad n = 0,1,2,3,\ldots,N-1. \tag{8}$$

Here, W_N represents the complex roots of unity used in the discrete Fourier transform (DFT) and $A[K]$ denotes the discrete Fourier transform of the N data points. The following explains how the inverse DFT (IDFT) reconstructs the original signal from these N transformed points:

$$a[k] = \frac{1}{N}\sum_{N=0}^{N-1} W_N^{-kn} \cdot A[n], \quad n = 0,1,2,3,\ldots,N-1. \tag{9}$$

Equation (8) indicates that each DFT value requires N complex multiplications and $N - 1$ additions, underscoring the computational intensity of the process and the necessity for more efficient algorithms such as FFT.

3.5 STFT

To ensure the accurate time-frequency representation of motor acoustic signals, in this study, we employed STFT for spectral analysis. STFT enables localized frequency analysis by segmenting the signal into fixed-length windows and applying the Fourier transform to each segment. This method is particularly effective in capturing time-dependent frequency variations in motor sounds, which are crucial for identifying anomalies such as bearing wear, misalignment, and gear friction noise.

Mathematical Representation of STFT

STFT is mathematically defined as

$$X(n,m) = \sum_{k=0}^{N-1} x(k)\, w(k-n)\, W_N^{mk}, \quad m = 0, L, N-1, \tag{10}$$

where N is the signal length, n is the shift in window function, $w(k)$ is the window function, L is the window length.

A 2048-sample Hamming window was selected for its optimal balance between frequency preservation and spectral leakage suppression. It outperformed the Hann and Blackman windows in resolution and distortion control, which are critical for fault detection. An ablation study confirmed its effectiveness in distinguishing faulty signals and enhancing feature robustness under varying speeds and loads.

3.6 MFCCs

In this study, MFCCs were used as a feature extraction method to analyze sound signals from car window motors. MFCCs are widely recognized for their ability to represent the spectral and perceptual properties of audio signals effectively, making them ideal for sound classification tasks. MFCCs transform raw acoustic signals into condensed feature sets, encapsulating essential characteristics while mitigating noise, as depicted in Fig. 16. This methodology

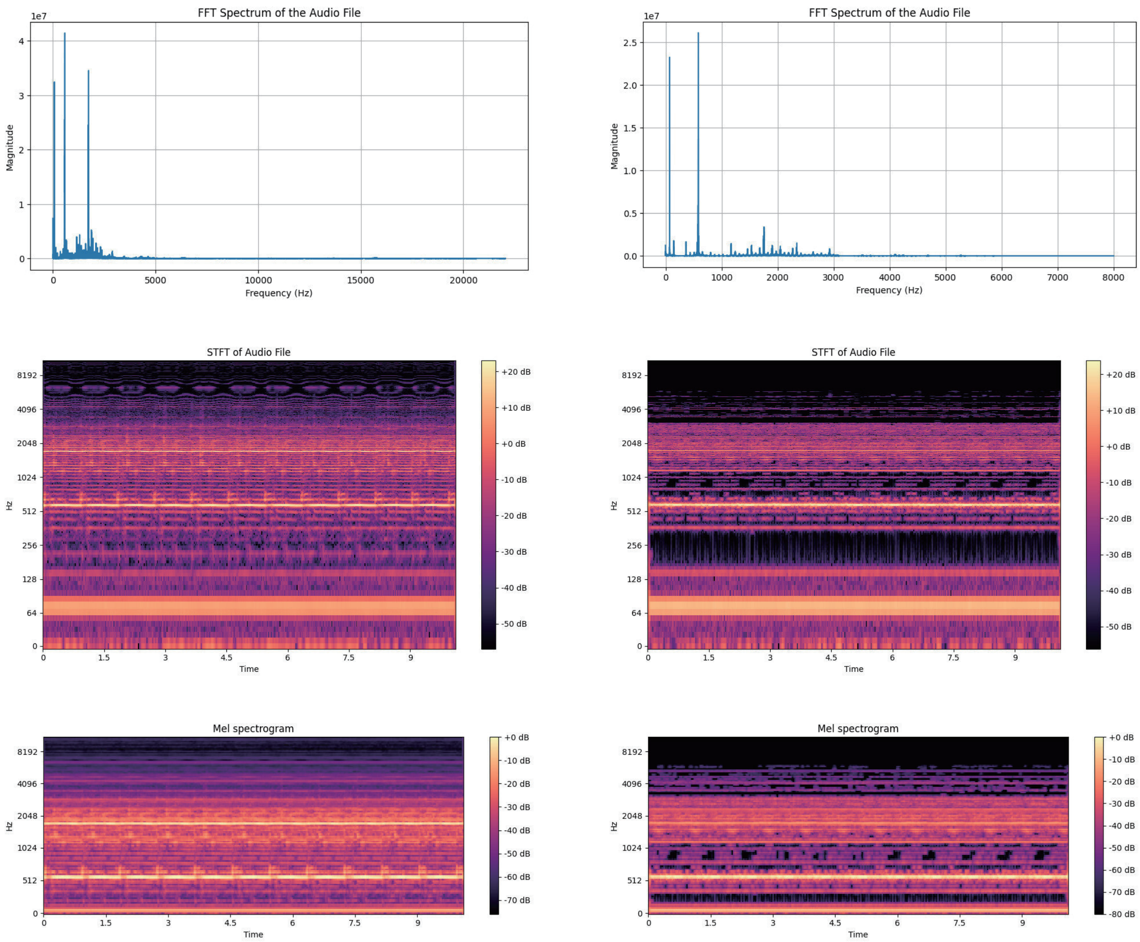

(a) (b)

Fig. 16. (Color) Comparative analyses of FFT spectrum, STFT, and Mel spectrogram for (a) GO and (b) NG motor sounds.

facilitates a robust comparison of the MTS and CNNs in the context of motor anomaly detection. A Mel spectrogram containing 128 filter banks was constructed to achieve high-resolution frequency representation, customized for the CNN2D-LSTM model. A selection of 13 MFCCs was made to retain crucial spectral attributes. Although Delta and Delta-Delta MFCCs, which are effective in capturing temporal variations, were not included, their inclusion may be considered in subsequent studies to further refine classification precision.

In this study, we employed MFCCs, FFT, and STFT to extract critical spectral and temporal features for motor sound analysis, aligning with the distinct processing requirements of the MTS and CNNs. STFT serves as a foundational transformation, converting time-domain signals into time-frequency representations, which then facilitate further feature extraction through FFT and MFCC computations. For the MTS, FFT and STFT are utilized to capture frequency-domain characteristics, with the spectral centroid method determining the FFT centroid threshold. This threshold is subsequently incorporated into the *MD* formula, quantifying deviations from normal operating conditions and enabling anomaly detection. For CNNs, MFCCs serve as direct input features, preserving both spectral and temporal patterns essential for deep-learning-based classification. Unlike Mel spectrograms, which are primarily used for visualization, the CNN model processes MFCC numerical representations, ensuring a more structured and high-dimensional feature set optimized for deep learning.

MFCCs are extracted from the STFT spectrogram through the application of a Mel filter bank to the power spectrum, followed by logarithmic compression and a discrete cosine transform (DCT). An analysis comparing MFCC- and STFT-based CNNs indicated that, whereas STFT provides intricate spectral resolution, MFCCs offer a more compact and efficient feature set suitable for classification tasks. Both FFT and STFT facilitate robust frequency analysis for multi-time series-based statistical modeling; however, MFCCs provide structured, high-dimensional features specifically optimized for CNN architectures. This method effectively establishes a balanced, interpretable, and efficient framework to detect motor abnormalities. Figure 17 shows the MFCC feature extraction process in the context of motor sound analysis.

4. Results and Discussion

Each of the 20 automotive window motors was subjected to recording over the course of 40 distinct sessions, with individual session durations of 10 s. To maintain sufficient temporal resolution, these recordings were subdivided into 1 s intervals, producing 10 audio segments per session. Considering the motor's functioning in both forward and reverse directions, the recording process encompassed a total of 800 sessions, culminating in 16000 audio segments. This segmentation methodology facilitated a comprehensive representation of acoustic behavior in various operational states, providing a robust dataset for model training and evaluation.

In this comparative analysis, the MTS used the *MD* to quantify deviations from normative conditions, whereas CNNs used spectrograms and temporal features for the classification of motor sounds. Despite the limited diversity of motors, both models demonstrated efficacy in

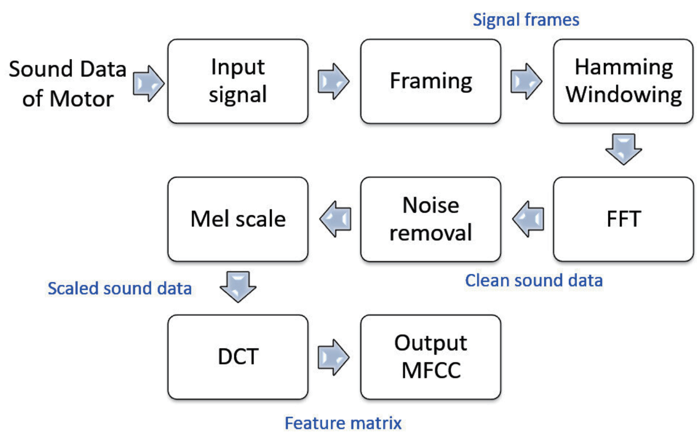

Fig. 17. (Color online) MFCC feature extraction for motor sound analysis.

distinguishing between normal and abnormal sounds. Future research will focus on enhancing the dataset to enhance the robustness and statistical dependability of the model. Figure 18 shows the workflow, from data acquisition to preprocessing and classification, highlighting a systematic methodology for feature extraction and anomaly detection in automotive motor diagnostics.

In this research, we used both the MTS and CNNs to examine acoustic emissions from vehicle window motors. Motor operation was managed by a LabVIEW-based system, with signals transmitted through a USB-2405 module and relay to facilitate forward and reverse motions. The DC motor generated low-speed linear movement (~20 mm/s), while a high-sensitivity microphone captured sound emissions. The audio was digitized at 44.1 kHz and stored as mono WAV files using LabVIEW, ensuring that the data maintained a high resolution for analysis. The complete system workflow is shown in Fig. 19, which describes the process from signal generation to data acquisition and storage.

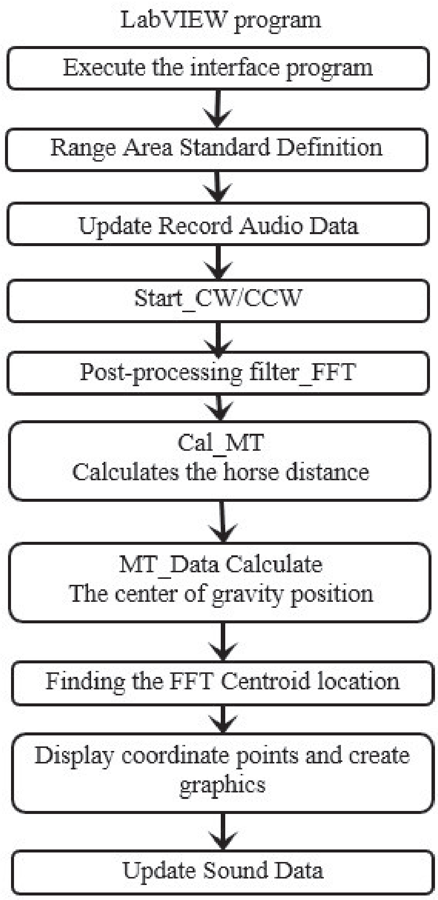

Fig. 18. Flowchart of motor sound recognition experiment using MTS.

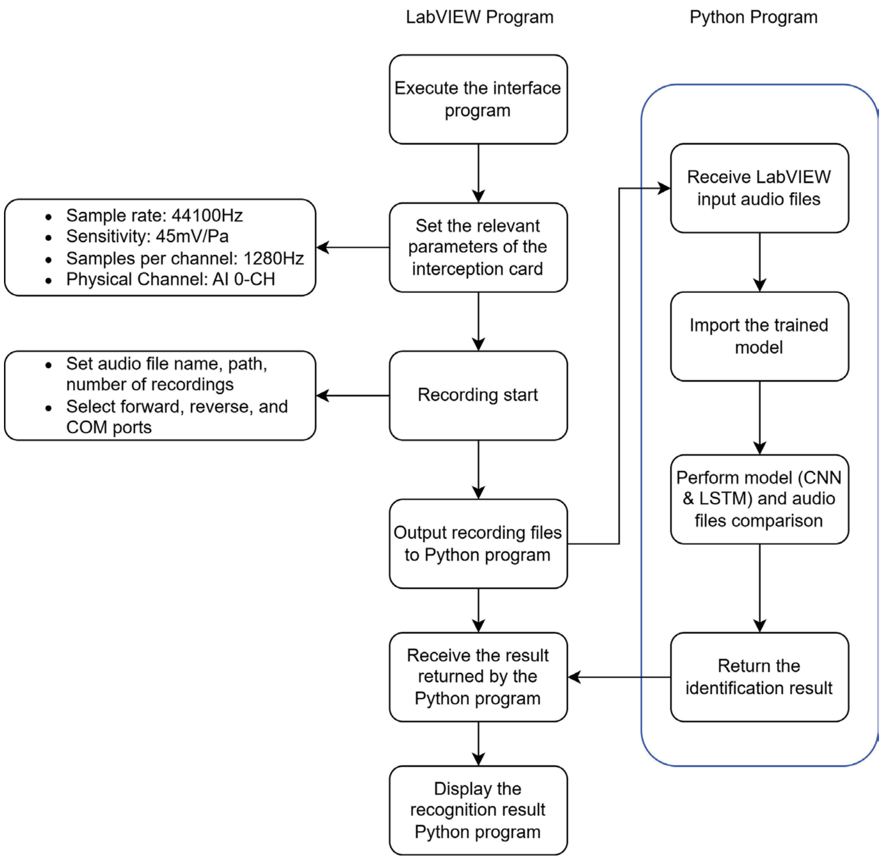

Fig. 19. (Color online) Flowchart of motor sound recognition experiment using CNNs.

4.1 Feature analysis and diagnostic output – MTS performance

In this study, the synchronization of acoustic data with the motor's operation was meticulously conducted to accurately represent its performance across diverse conditions. The recognition software acquired sound over a two-second duration per session and then applied FFT analysis to extract features within the frequency domain. FFT facilitated the examination of the motor sound's frequency characteristics. Critical data, such as the center of gravity frequency, were preserved for further analysis. As depicted in Fig. 20, the system identified the peak frequency and amplitude values, implementing a root mean square (*RMS*) calculation for each interval to produce characteristic values for subsequent evaluation. Furthermore, to assess the consistency and detect anomalies in the extracted features, *MD* analysis was conducted to quantify deviations from the normal operating patterns by considering correlations among multiple variables. This approach provided a robust method for identifying both minor and severe anomalies in the motor's performance.

To examine the dynamic frequency characteristics of motor sounds, FFT was employed to evaluate sound pressure fluctuations, thus offering a comprehensive acoustic profile conducive to precise diagnostics. The outcome of the MTS was juxtaposed with that of CNNs in the context of anomaly detection. The data acquisition system facilitated real-time evaluation, initiated via

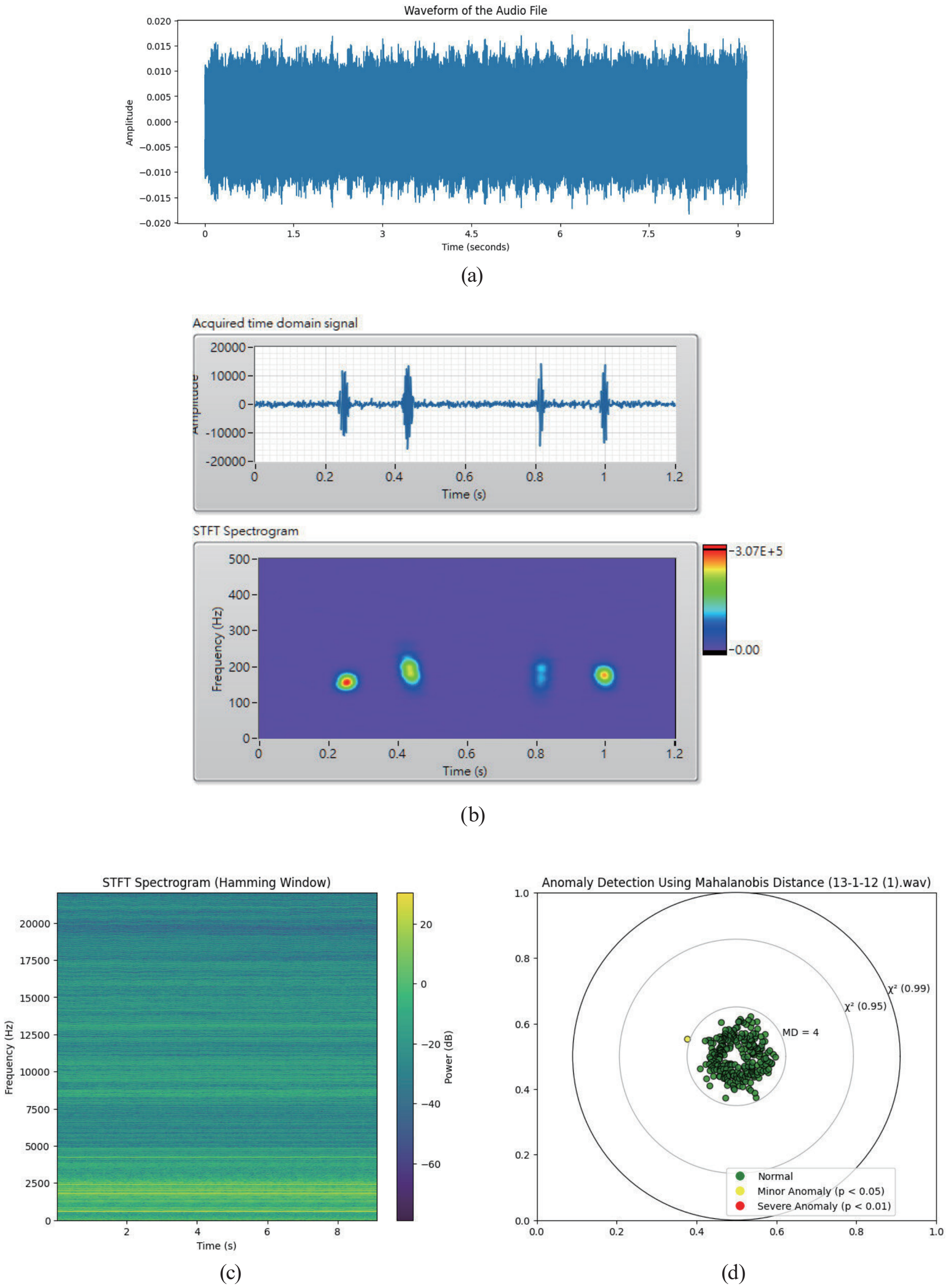

Fig. 20. (Color online) (a) Analysis curves of sound signal, (b) FFT frequency, (c) STFT frequency, and (d) MD analysis.

the ‘DAQ Start’ button, which ensured the adherence of the signal to established parameters. As illustrated in Fig. 21, the results were visualized using color-coded dots: green indicated normality, yellow signified a warning (5% deviation), and red denoted abnormality (1% deviation), thus allowing the prompt identification of motor faults.

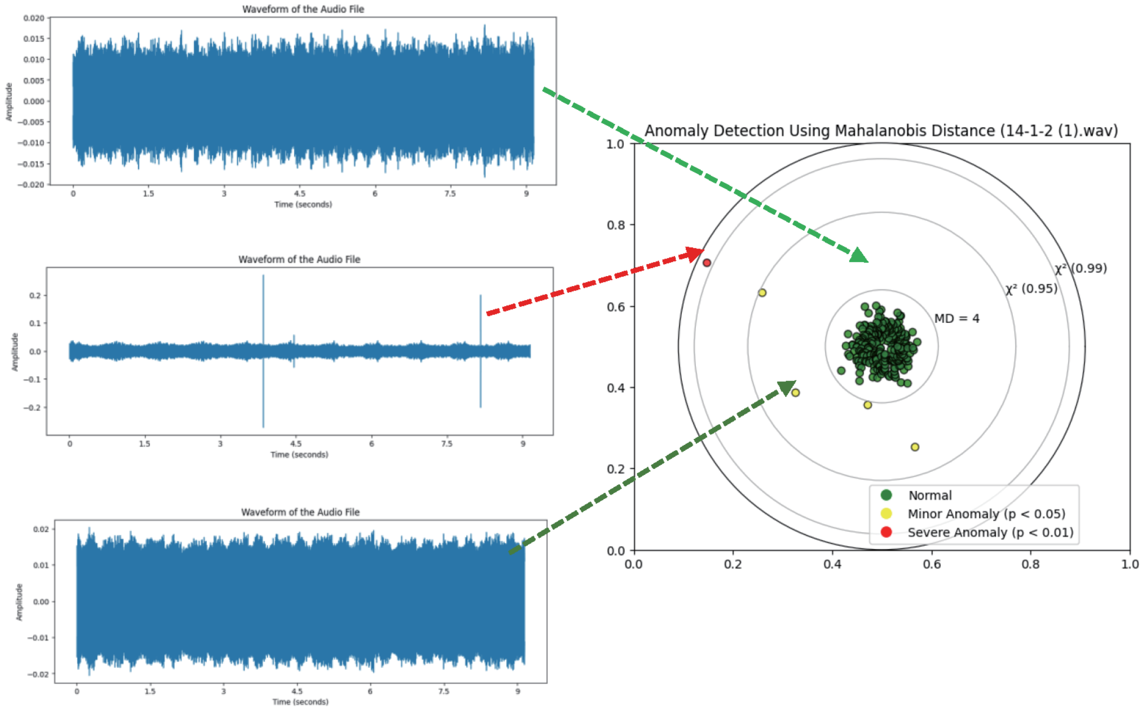

Fig. 21. (Color) Motor recognition system verification chart: (a) green dots: GO and (b) red dots: NG.

4.2 CNN performance and spectrogram-based fault detection

Motor acoustic signals were analyzed using CNNs, which leveraged features extracted from both the temporal and spectral domains for anomaly detection. In the temporal domain, waveform analysis revealed patterns related to periodicity and amplitude variations. As shown in Figs. 22 and 23, the waveform associated with the GO (normal) motor exhibited consistent and stable patterns, whereas the NG (abnormal) motor demonstrated irregular and unstable fluctuations. These observations suggest that waveform characteristics serve as effective indicators for distinguishing between normal and abnormal motor conditions, indicative of potential problems such as increased friction or structural faults. Spectral domain analysis by applying FFT and STFT facilitates the identification of frequency characteristics essential to fault diagnosis. In Fig. 22 (GO), a consistent frequency distribution is observed, while Fig. 23 (NG) presents deviations at approximately 3, 5, and 8 s, characterized by vertical spectral disturbances and elevated energy within the 2–5 kHz range, indicative of potential mechanical issues such as gear misalignment or wear. CNNs proficiently identify such anomalies by recognizing frequency deviations and transient patterns. When contrasted with MTS models that use the *MD*, CNNs exhibit superior accuracy, as they more effectively capture subtle spectral variations. Consequently, deep-learning-based spectrogram analysis advances diagnostic reliability, positioning CNNs as a robust instrument for automated motor fault detection.

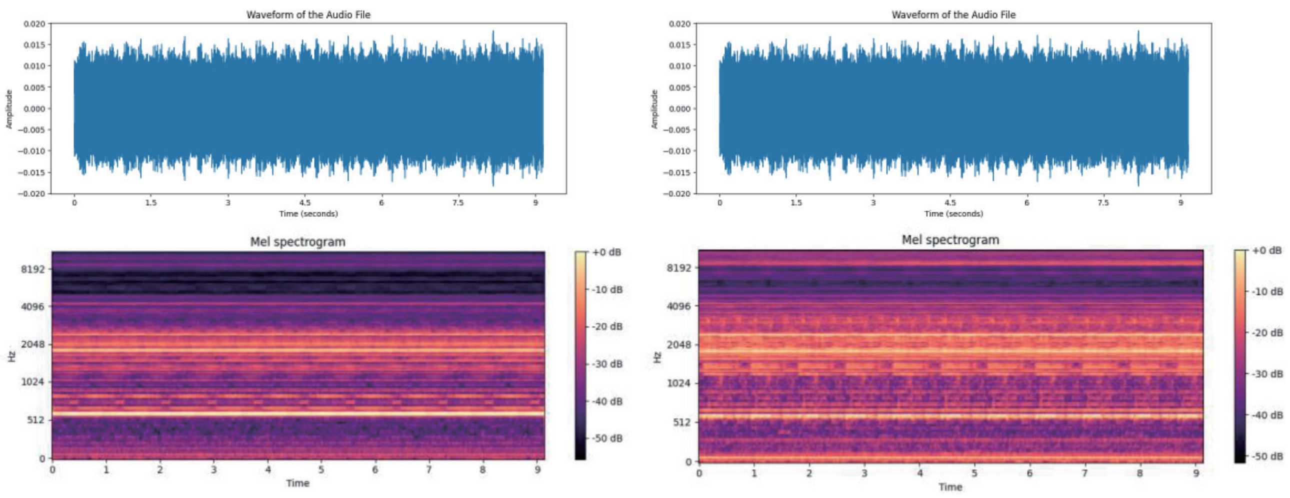

Fig. 22. (Color online) GO spectrum sound signal graph.

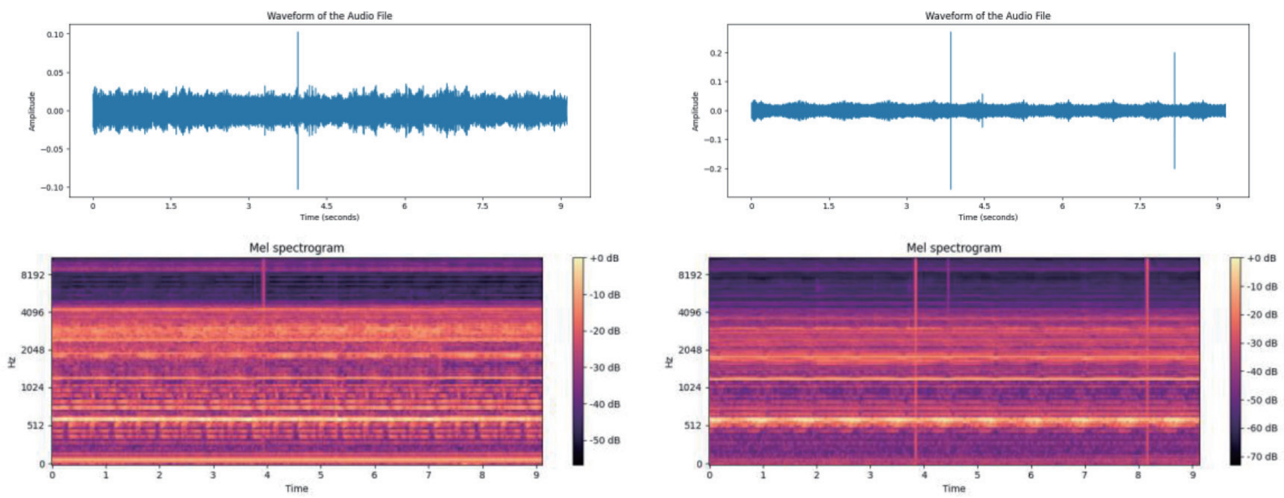

Fig. 23. (Color) NO GO spectrum sound signal graph.

The CNN-LSTM model outperformed the MTS approach in motor anomaly detection, effectively combining convolutional feature extraction with temporal modeling. Trained on a 70/30 train–test split and optimized through hyperparameter tuning, the model achieved an accuracy of 93.1% [Fig. 24(a)] and a final loss of 0.116, indicating stable convergence and minimal overfitting. Validation on 800 unseen samples yielded a recognition rate of 97%, confirming strong generalization across varying motor conditions. The confusion matrix is shown in Fig. 24(b).

Comparative training evaluations revealed that CNNs achieved an accuracy rate of 98% with rapid convergence, whereas CNN-LSTM exhibited a marginally lower convergence rate, which can be ascribed to its elevated complexity. To enhance the generalization capabilities of the

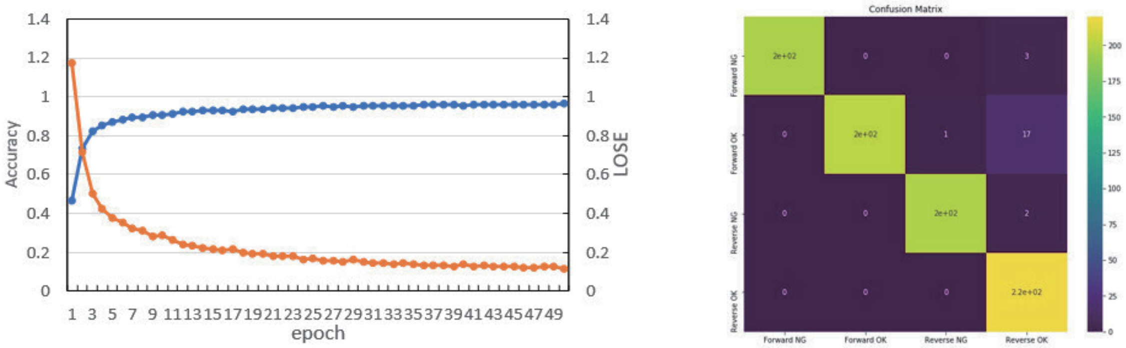

(a) (b)

Fig. 24. (Color online) (a) CNN method accuracy and loss rate of model training results and (b) confusion matrix.

model, measures such as a 30% dropout rate, L2 regularization (λ = 0.001), early stopping mechanisms, and adaptive learning rate adjustments were used. The CNN-LSTM model attained an accuracy of 96.6%, as shown in Fig. 25(a), with the confusion matrix depicted in Fig. 25(b) corroborating its high precision in distinguishing between normal and defective motors. These findings highlight the efficacy of the model in encapsulating temporal and spectral attributes. It is recommended to further substantiate these observations through the analyses of the accuracy and trends of loss of the test to evaluate its practical applicability.

4.3 Comparative evaluation of CNN-LSTM and MTS models for motor anomaly detection

The CNN-LSTM model demonstrated superior performance compared with the MTS in the domain of motor anomaly detection, achieving an accuracy rate of 96.6%. This result was particularly evident in the enhancement of identifying functional (GO) motors. The model's capacity to assimilate both spectral and temporal characteristics augmented the detection of minute sound variations. The statistical validity of its enhanced performance was corroborated by McNemar's test (p = 0.0034), which affirmed the robustness of the CNN-based approach. Conversely, although the MTS attained an accuracy of 100% in the identification of defective (NG) motors, its performance was limited to an accuracy of 86.6% for GO motors. This limitation reflects its constraints in distinguishing subtle differences in acoustic signatures, subsequently resulting in a heightened false positive rate. Nevertheless, owing to its reduced computational complexity, the MTS remains beneficial in environments with constrained resources, rendering it a practical alternative for real-time edge computing applications.

The CNN-LSTM model demonstrated a precision of 94.3% and a recall of 90.5%, underscoring its efficacy in detecting motor abnormalities for predictive maintenance purposes. As presented in Table 5, CNN2D + LSTM surpasses the MTS in all essential metrics, including accuracy, precision, recall, and F1 score. Future research will be directed towards augmenting the dataset to improve generalizability and investigating hybrid models that integrate CNN feature extraction with MTS analysis to advance diagnostic accuracy and efficiency.

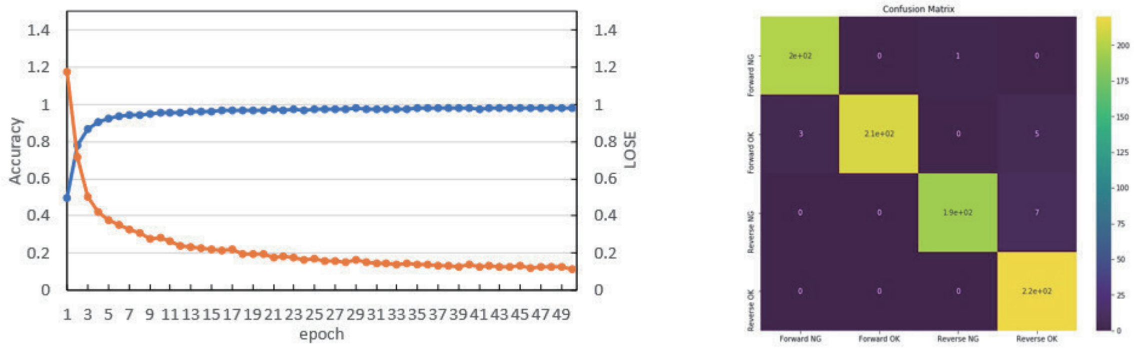

(a) (b)

Fig. 25. (Color online) (a) CNN+LSTM method accuracy and loss rate of model training results and (b) confusion matrix.

Table 5
Performance comparison of CNN2D+LSTM and MTS in motor anomaly detection.

Model	Accuracy (%)	Precision (%)	Recall (%)	F1-score (%)	*p*-value (McNemar's test)
CNN2D+LSTM	96.6	94.3	90.5	92.3	0.0034 (Significant)
MTS	86.6	85.1	81.8	83.4	–

5. Conclusion

In this study, we conducted a comparative analysis of the sophisticated MTS and CNNs in the detection of abnormal acoustic emissions in automotive window motors. The objective was to develop an intelligent auditory system capable of distinguishing functional motors (GO) from defective motors (NO GO), thus reducing the dependence on manual inspection. When signal processing was integrated with machine learning techniques, an automated acoustic recognition platform was formulated. The experimental findings indicated that the Conv2D+LSTM model attained an accuracy of 96.6%, surpassing the MTS accuracy of 86.6%. CNNs demonstrated superior effectiveness in managing spectrogram data and capturing temporal patterns, exhibiting higher precision and recall. This makes them highly suitable for applications in predictive maintenance and quality control.

Although the proposed system demonstrates promising results, further improvements are required to optimize adaptability and robustness. Subsequent research efforts will focus on broadening the dataset to encompass a more extensive array of motor conditions, thereby augmenting generalization. The investigation of hybrid deep learning models that integrate CNNs with anomaly detection methodologies is expected to enhance diagnostic accuracy. Furthermore, the inclusion of predictive modeling is expected to facilitate early fault detection, significantly advancing intelligent manufacturing and industrial automation.

The implementation of machine learning and artificial intelligence in sound-based anomaly detection lays a foundational framework for advanced quality control solutions within industrial manufacturing. In this study, the proficient application of CNN-based acoustic recognition underscores its transformative potential in predictive maintenance, thus reducing operational downtime, improving product reliability, and bolstering manufacturing efficiency. Anticipated progress in data augmentation, lightweight architectures, and multimodal fusion—such as the integration of vibration and electrical signal monitoring with CNNs and the MTS—is projected to further strengthen the robustness of the system, making it a feasible solution for large-scale industrial applications. Furthermore, the expansion of datasets and the implementation of real-world validation within production settings will facilitate standardized evaluation and improve generalization under diverse motor conditions.

Acknowledgments

The authors sincerely express their gratitude to the Ministry of Science and Technology for the financial support under grant number NSTC 113-2221-E-224-027.

References

1 K. Stylidis, S. Hoffenson, C. Wickman, M. Söderman, and R. Söderberg: Procedia CIRP **21** (2014) 171. https://doi.org/10.1016/j.procir.2014.03.144
2 K. Stylidis, C. Wickman, and R. Söderberg: Procedia CIRP **36** (2015) 165. https://doi.org/10.1016/j.procir.2015.01.076
3 M. d. Pardo-Ferreira, J. C. Rubio-Romero, F. C. Galindo-Reyes, and A. Lopez-Arquillos: Saf. Sci. **121** (2020) 580. https://doi.org/10.1016/j.ssci.2019.02.021
4 G. Pietila, and T. C. Lim: Appl. Acoust. **73** (2012) 987. https://doi.org/10.1016/j.apacoust.2012.04.012
5 J.-Y. Kim, and S.-B. Cho: Neurocomputing **452** (2021) 395. https://doi.org/10.1016/j.neucom.2019.10.123
6 X. Zheng, Q. Zhou, Z. Hao, and Y. Qiu: Appl. Acoust. **171** (2021) 107670. https://doi.org/10.1016/j.apacoust.2020.107670
7 V. G. C. Cook and A. Ali: Appl. Acoust. **73** (2012) 265. https://doi.org/10.1016/j.apacoust.2011.06.019
8 C. Y. Cheng, J. C. Renn, C. E. Shi, and I. Saputra: Proc. 2022 19th Int. Conf. Automation Technology (Automation 2022) 1–8.
9 O. S. Bhosale, D. Huajrea, and M. S. Laila: Noise Vibr. Worldwide **53** (2022) 428. https://doi.org/10.1177/09574565221128061
10 O. Marinov, M. J. Deen, J. A. Jiménez-Tejada: Phys. Rep. **990** (2022) 1. https://doi.org/10.1016/j.physrep.2022.06.005
11 K. C. Kim, S. W. Lee, S. G. Hong, J. Kim, G. J. Lee, J. M. Choi, and Y. J. Kim: SAE Int. 2015-01-2257 (2015) 1. https://doi.org/10.4271/2015-01-2257
12 L. Rojas, Á. Peña, and J. Garcia: Appl. Sci. **15** (2025) 3337. https://doi.org/10.3390/app15063337
13 F. Akbalık, A. Yıldız, Ö. F. Ertuğrul, and H. Zan: Appl. Sci. **14** (2024) 6532. https://doi.org/10.3390/app14156532
14 E. Di Fiore, A. Ferraro. A. Galli, V. Moscato, and G. Sperlì: Expert Syst. Appl. **209** (2022) 118324. https://doi.org/10.1016/j.eswa.2022.118324
15 C. F. Chi, R. S. Dewi, Y. Y. Surbakti, and D. Y. Hsieh: Ergonomics **60** (2017) 1471. https://doi.org/10.1080/00140139.2017.1323121
16 K. K. M. Shariff, R. Raju, I. Yassin, F. Eskandari, and M. S. A. M. Ali: Qeios. (2023) GCHCCC. https://doi.org/10.32388/GCHCCC
17 M. Yang, P. Dai, Y. Yin, D. Wang, Y. Wang, and H. Huang: ISA Trans. **157** (2025) 556. https://doi.org/10.1016/j.isatra.2024.11.059
18 Z. Yang, S. Ye, Z. Wang, Z. Li, and W. Li: Eng. Fail. Anal. **145** (2023) 107017. https://doi.org/10.1016/j.engfailanal.2022.107017
19 M. Jarnut, J. Kaniewski, and M. Buciakowski: Energies **18** (2025) 778. https://doi.org/10.3390/en18040778
20 L. Kong, X. Zhao, X. Yuan, Q. Yu, P. Shi, C. Zhou, and D. Zhang: Mech. Syst. Signal Process. **223** (2025) 111919. https://doi.org/10.1016/j.ymssp.2024.111919

21 C. Y. Cheng, J. C. Renn, I. Saputra, and C. E. Shi: Int. J. Mech. Eng. Robot Res. **11** (2022) 737. https://doi.org/10.18178/ijmerr.11.10.737-744
22 C. Eang and S. Lee: Sensors **25** (2024) 25. https://doi.org/10.3390/s25010025
23 F. Ramlie, W. Z. A. W. Muhamad, N. Harudin, M. Y. Abu, H. Yahaya, K. R. Jamaludin, and H. H. A. Talib: Appl. Sci. **11** (2021) 3906. https://doi.org/10.3390/app11093906
24 C. F. Peng, L. H. Ho, S. B. Tsai, Y. C. Hsiao, Y. Zhai, Q. Chen, L. C. Chang, and Z. Shang: Sustainability **9** (2017) 1557. https://doi.org/10.3390/su9091557
25 N. N. N. M. Kamil, M. Y. Abu, N. F. Zamrud, F. L. M. Safeiee, and M. Oktaviandri: J. Phys. Conf. Ser. **1532** (2020) 012004. https://doi.org/10.1088/1742-6596/1532/1/012004
26 R. Espinosa, H. Ponce, and S. Gutiérrez: Appl. Soft Comput. **108** (2021) 107465. https://doi.org/10.1016/j.asoc.2021.107465
27 R. You, Q. Tao, S. Wang, L. Cao, K. Zeng, J. Lin, and H. Chen: Bioengineering **12** (2025) 238. https://doi.org/10.3390/bioengineering12030238
28 J. Hou, H. Yi, X. Xiang, X. Ni, R. Dai, and X. Huang: Sound Vib. **59** (2025) 1941. https://doi.org/10.59400/sv1941
29 H. Jung, S. Choi, and B. Lee: Electronics **12** (2023) 480. https://doi.org/10.3390/electronics12030480
30 Y. Gonzales and R. C. Prati: Electronics **11** (2022) 1405. https://doi.org/10.3390/electronics11091405
31 X. Yin, Q. He, H. Zhang, Z. Qin, and B. Zhang: Electronics. **11** (2022) 2422. https://doi.org/10.3390/electronics11152422
32 H. B. Huang, R. X. Li, X. R. Huang, T. C. Lim, and W. P. Ding: Appl. Acoust. **113** (2016) 137. https://doi.org/10.1016/j.apacoust.2016.06.016
33 M. M. Osman and O. Büyük: Sigma J. Eng. Nat. Sci. **38** (2020) 2177.

About the Authors

Chin-Yi Cheng received his B.Eng. degree in mechanical engineering from National Yunlin University of Science and Technology (NYUST), Taiwan in 2008. He received his M.Sc. and Ph.D. degrees in Mechanical Engineering from NYUST, Douliu in 2010 and 2014, respectively. He continued to work as a postdoctoral researcher at NYUST for two more years after receiving his Ph.D. degree. After his postdoctoral work, he became an assistant professor in the Mechanical Engineering Department of NYUST. His current research interests are in the design of fluid transmission and system control, smart mobile vehicles, electromagnetic simulation analysis, CFD simulation, and AI industrial control system development. (zezheng@yuntech.edu.tw)